Journal of Materials Chemistry B

ROYAL SOCIETY OF CHEMISTRY

PAPER

View Article Online
View Journal | View Issue

Cite this: J. Mater. Chem. B, 2021, 9, 8646

Heterogenous hydrogel mimicking the osteochondral ECM applied to tissue regeneration†

Zhuoxin Chen,‡[a] Hong Xiao,‡[b] Hongbo Zhang,[a] Qiangwei Xin,[a] Haochen Zhang,[a] Haixin Liu,[c] Mingzhen Wu,[a] Liangrui Zuo,[a] Jun Luo,[a] Qiang Guo,[d] Chunmei Ding,*[ae] Hong Tan[a] and Jianshu Li*[adf]

Received 10th March 2021,
Accepted 9th September 2021

DOI: 10.1039/d1tb00518a

rsc.li/materials-b

Inspired by the intricate extracellular matrix (ECM) of natural cartilage and subchondral bone, a heterogenous bilayer hydrogel scaffold is fabricated. Gelatin methacrylate (GelMA) and acryloyl glucosamine (AGA) serve as the main components in the upper layer, mimicking the chondral ECM. Meanwhile, vinylphosphonic acid (VPA) as a non-collagen protein analogue is incorporated into the bottom layer to induce the *in situ* biomineralization of calcium phosphate. The two heterogenous layers are effectively sutured together by the inter-diffusion between the upper and bottom layer hydrogels, together with chelation between the calcium ions and alginate added to separate layers. The interfacial bonding between the two different layers was thoroughly investigated *via* rheological measurements. The incorporation of AGA promotes chondrocytes to produce collagen type II and glycosaminoglycans and upregulates the expression of chondrogenesis-related genes. In addition, the minerals induced by VPA facilitate the osteogenesis of bone marrow mesenchymal stem cells (BMSCs). *In vivo* evaluation confirms the biocompatibility of the scaffold with minor inflammation and confirms the best repair ability of the bilayer hydrogel. This cell-free, cost-effective and efficient hydrogel shows great potential for osteochondral repair and inspires the design of other tissue-engineering scaffolds.

Introduction

Osteochondral defects are regarded as a tough problem with lesions ranging from articular cartilage to the underlying subchondral bone,[1] which can affect people of all ages.[2] The challenge for the treatment of osteochondral defects lies in two aspects: on the one hand, the composition, structure and cells differ significantly between the articular cartilage and the subchondral bone;[3] on the other hand, the avascular nature of cartilage largely limits its capability of regeneration. Given the heterogenous nature of the osteochondral area, conventional monophasic scaffolds are incapable of repairing the complicated tissue with its corresponding functions and structrues.[4] By contrast, the heterogenous bilayer scaffold can be well designed to integrate remarkably different structural and mechanical properties within the whole material.[5] This strategy generates a local microenvironment similar to that of natural tissue, and has been studied greatly in recent decades.[6,7] Moreover, for the effective regeneration of defect tissue, cells and growth factors are commonly introduced. For instance, bone marrow mesenchymal stem cells (BMSCs),[8,9] bone morphology protein-2 (BMP-2) and transforming growth factor-β1 (TGF-β1) are often utilized to increase the bioactivity of

[a] College of Polymer Science and Engineering, State Key Laboratory of Polymer Materials Engineering, Sichuan University, Chengdu 610065, China. E-mail: dingcm@scu.edu.cn, jianshu_li@scu.edu.cn
[b] Department of Pain Management, West China Hospital, Sichuan University, No. 37, GuoXue Xiang, Chengdu 610041, China
[c] Department of Orthopedics, People's Hospital of Deyang City, No. 173, Taishan North Road, Deyang 618000, China
[d] State Key Laboratory of Oral Diseases, West China Hospital of Stomatology, Sichuan University, Chengdu 610041, China
[e] CAS Key Laboratory of Bio-inspired Materials and Interfacial Science, Technical Institute of Physics and Chemistry, Beijing 100190, China
[f] Med-X Center for Materials, Sichuan University, 610041, China

† Electronic supplementary information (ESI) available: Hydrogel formulas for *in vitro* cell study, the sequences of primers used for real-time PCR, frequency sweeps for hydrogels of different groups, photographs and swelling ratios of hydrogels, SEM images of double-layer hydrogels of different sites, fluorescence microscopy images of chondrocytes cultured on upper layers of hydrogels for 7 days, body weights of SD rats in different groups post-surgery, scores of H&E stains in subcutaneous tissue, 3D reconstruction of samples of different groups, the reconstructed VOI images of defect areas for different groups, bone volume/total volume (BV/TV), bone mineral density of total volume (BMD of TV), and bone mineral density of bone volume (BMD of BV) calculated from micro-CT results, and collagen-I and collagen-II stains of collected knee joints after 6 weeks of implantation. See DOI: 10.1039/d1tb00518a

‡ Zhuoxin Chen and Hong Xiao contributed equally to this work.

scaffolds and promote restoration.[10,11] However, the incorporation of these bioactive components is troublesome and expensive, which could induce great difficulty for practical clinical translation. In general, cost effectiveness and cell-free approaches are preferentially demanded.[12]

The physiochemical properties of the scaffold, such as the composition and stiffness, are vital to the cell behaviour and are usually engineered to allow tissue regeneration by the manipulation of the cell fate.[13] The intricate ECM of natural cartilage and subchondral bone inspires the choice of materials. For the cartilage layer, chondrocytes are located in the gel-like ECM with the main components of collagen, glycosaminoglycans (GAGs), proteoglycan and water;[14] however, for the subchondral layer, aside from collagen, calcium phosphates (CaPs) induced by organic proteins and cells constitute the majority of the ECM.[15] In light of this, double-layer hydrogels with the components of collagen (or gelatin), GAGs and CaPs have been technically constructed to simulate the natural ECM.[5] Although large efforts have been made, the regeneration of articular cartilage has been far from satisfactory. As a consequence, it is of great significance to discover materials that are beneficial for cartilage repair. Moreover, in particular, the favourable stiffness for chondrogenic and osteogenic differentiation of BMSCs shows a large difference.[16] With regard to this, bilayer hydrogels are normally constituted by a soft cartilaginous layer and a stiff subchondral bone layer.[17] Nevertheless, it remains a great challenge to realize stable interfacial bonding between two layers that have a different composition and stiffness.

Aiming at the above two problems, we attempt to design heterogenous bilayer hydrogels with a robust interfacial bonding strength and a local environment that is favourable for osteochondral defect repair, especially the restoration of articular cartilage. Glucosamine is a fundamental constituent of GAGs and forms the basic moieties of saccharides. Very recently, our group has found the positive role of these moieties for the chondrogenic differentiation of BMSCs.[18] Furthermore, glucosamine also possesses the ability to prevent joint space narrowing[19] and can enhance chondrogenesis.[20] On the basis of this, it is reasonable to expect the advantageous effect of glucosamine for cartilage regeneration, which is rarely investigated nowadays. Herein, gelatin methacrylate (GelMA) and acryloyl glucosamine (AGA) are incorporated as ECM mimetics of the upper cartilage layer (collagen and glucosamine). Meanwhile, to afford CaPs in the bottom layer, vinylphosphonic acid (VPA), as an NCP analogy, is adopted to induce the biomineralization of CaPs by abundant phosphate groups, as referred to in our previous work.[21] The incorporation of CaPs improves the stiffness of the bottom layer of the hydrogel, and is beneficial for bone regeneration. Moreover, the two layers with diverse compositions and mechanical properties were sutured into an intact layer by delicate control of the interdiffusion between the upper and bottom layer hydrogels, together with the chelation between calcium ions and alginate added to the separate layers (Scheme 1). The physicochemical properties of the monomers and hydrogels were investigated. Cell experiments with chondrocytes and BMSCs were conducted on the upper and bottom layers, respectively. Moreover, the repair of osteochondral defects was evaluated *in vivo*.

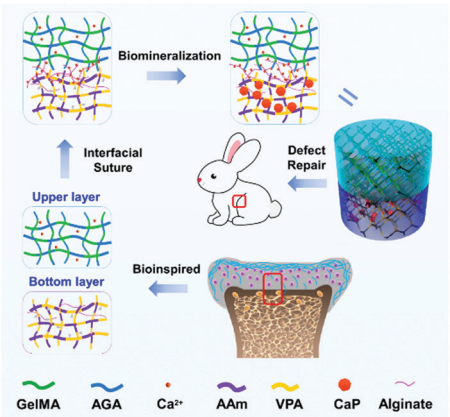

Scheme 1 Schematic illustration showing the ECM-inspired double-layer hydrogel for the repair of osteochondral defects.

Experimental

Chemicals and materials

Gelatin (from porcine skin), methacrylic anhydride and acryloyl chloride were purchased from Sigma Aldrich. D-Glucosamine hydrochloride was obtained from Yuanye Biotechnology Co., Ltd. Irgacure 2959 was acquired from BASF Corporation. Streptomycin, penicillin, trypsin, alfa-minimum essential medium (α-MEM) and Dulbecco's modified Eagle's medium (DMEM) were purchased from Chengdu Bosco Biotechnology Co. Ltd. The alkaline phosphatase (ALP) kit and the bicinchoninic acid (BCA) kit were obtained from Shanghai Beyotime Biotechnology, Co., Ltd. The rat glycosaminoglycan (GAG) ELISA kit, rat collagen type I (Col-I) and type II (Col-II) ELISA kits, rat interleukin 1β (IL-1β) ELISA kit, rat interleukin6 (IL-6) ELISA kit and rat tumor necrosis factor α (TNF-α) ELISA kit were commercially available from Bio-swamp Life Science Lab. Rhodamine phalloidin and 4′,6-diamidino-2-phenylindole (DAPI) stains were bought from Solarbio Life Sciences Company. Other chemicals unless otherwise mentioned were purchased from Haihong Chemical Company (Chengdu, China).

Synthesis of monomers

The synthesis of GelMA and AGA was carried out as previously described[22,23] with slight modification. Briefly, for the acrylation of gelatin (Fig. 1a), gelatin (2.5 g) was dissolved in phosphate buffered saline (PBS, 25 mL) at the temperature of 50 °C, followed by the addition of methacrylic anhydride (5 mL) at a rate of 0.5 mL min^{-1}. The reaction lasted for 1 h at 50 °C and was stopped by 5-times dilution with PBS. The diluted solution was then transferred to a 12–14 kDa dialysis tube and dialyzed against water for 1 week at 50 °C to remove the salts and other impurities. After that the solution was lyophilized for

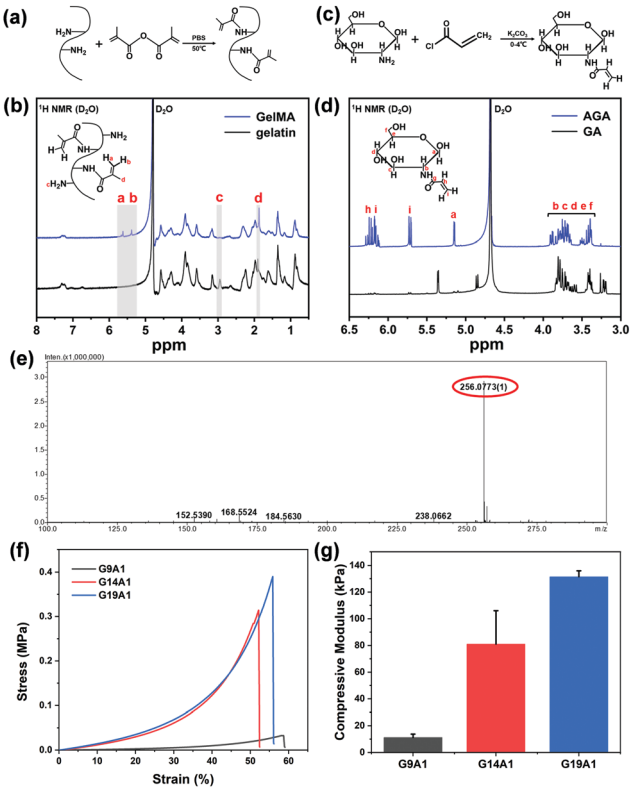

Fig. 1 (a) The synthesis process of gelatin methacrylate (GelMA), (b) ^{1}H NMR spectra of gelatin before and after modification, (c) the synthesis process of acylated glucosamine (AGA), (d) ^{1}H NMR spectra of native glucosamine and AGA, (e) mass spectrum of AGA, (f) the stress–strain curves of G9A1, G14A1 and G19A1, and (g) the compressive moduli of G9A1, G14A1 and G19A1.

1 week to obtain a porous, white, foam-like substance which was stored at −20 °C before use.

For the synthesis of AGA (Fig. 1c), glucosamine (GA, 0.02 mol) was dissolved in 1 M K_2CO_3 solution (20 mL). Acryloyl chloride (0.024 mol) was added dropwise to the solution at −4 °C for the reaction for 4 hours in the dark; after this, the whole solution was then allowed to evaporate at room temperature for 24 hours to remove the unreacted acryloyl chloride. The as-prepared mixture was dissolved in water, lyophilized and purified using silica column chromatography. Finally, the obtained solution was lyophilized again and stored at −20 °C.

Characterization of monomers

^{1}H nuclear magnetic resonance (^{1}H NMR; AV III HD 400 MHz, Bruker, Germany) was utilized to examine the gelatin and glucosamine before and after modification. Electrospray mass spectroscopy (MS; Finnigan TSQ Quantum Ultra, Thermo Fisher Scientific, USA) was applied to analyse the molecular weight of the modified glucosamine. To calculate the substitution degree of the free amino groups in the gelatin molecule, the *ortho*-phthalaldehyde (OPA) method[24] was adopted. In short, 40 mg of OPA was dissolved in 1 mL of methanol, and then mixed with 2.5 mL of an SDS solution (20 wt%), 25 mL of borax solution (0.1 M) and 100 μL of β-mercaptoethanol. The obtained solution was diluted to 50 mL and used immediately. 200 μL of different concentrations of gelatin and the modified gelatin solution were added to 4 mL of the OPA solution for the reaction for 2 min at room temperature. The mixture was then examined using UV-vis spectrophotometry (UV-1800PC, APADA, China) at the wavelength of 340 nm. The degree of substitution (DS) was calculated by comparing the slope of the standard curve (k_{gelatin}) with that of the experimental curve ($k_{\text{modified gelatin}}$).

$$\text{DS} = (1 - k_{\text{modified gelatin}}/k_{\text{gelatin}}) \times 100\% \quad (1)$$

Preparation of bilayer hydrogel

The bilayer hydrogel was prepared by a two-step UV curing method. In short, acrylamide (AAm) and VPA were dissolved in 1 wt% sodium alginate solution with concentrations of 13.5 wt% and 1.5 wt%, respectively. *N*,*N*-Methylenebisacrylamide (MBAA, 1 wt%) was added to the solution as the crosslinker, followed by the addition of the photo-initiator Irgacure 2959 (0.5 wt%). The obtained mixture, as the precursor solution of the bottom-layer hydrogel, was degassed and transferred to PTFE moulds with different depths and diameters. The solution was pre-cured using UV irradiation for different time intervals (3, 5 and 7 min) to choose an optimal condition for bonding with the upper layer.

Meanwhile, GelMA and AGA with different concentrations were dissolved in deionized water (DIW), with the addition of Irgacure 2959 (0.5 wt%) and $CaCl_2$ (100 mM) as the precursor solution of the upper-layer hydrogel. The concentrations of GelMA and AGA were regulated as: G9A1–GelMA (13.5 wt%) and AGA (1.5 wt%), G14A1–GelMA (14 wt%) and AGA (1 wt%), and G19A1–GelMA (14.25 wt%) and AGA (0.75 wt%). After degassing, the solution was poured on the top of the bottom-layer solution, which had been pre-cured for 3, 5 and 7 min. The whole system was then exposed to UV light at the wavelength of 365 nm (1000 W) for 20 min. After curing, the bilayer hydrogels with different sizes were obtained. For the preparation of single-layer hydrogels, the mould was filled with either the upper- or bottom-layer hydrogel precursor solution and cured under the same conditions as for the bilayer hydrogels.

To investigate the effect of interfacial chelation (sodium alginate–Ca^{2+}) on the rheological properties, the upper-, bottom- and double-layer hydrogels were also prepared similarly as above, except that the sodium alginate and $CaCl_2$ were not added.

Mineralization of the bottom-layer hydrogel

Mineralization of the hydrogels was similar to previously reported in the literature.[25] The Ca/P metastable solution was prepared by adding 0.548 g of $K_2HPO_4{\cdot}3H_2O$ and 0.444 g of $CaCl_2$ to 70 mL of DIW. The obtained white turbid liquid became transparent after the slow addition of HCl (6 M). Tris–HCl (1 M, pH = 7.5) was then utilized to adjust the pH to 5.2, and afterwards the solution was diluted to 100 mL. The modified simulated body fluid (mSBF) was constituted by NaCl

(2.702 g), $NaHCO_3$ (0.252 g), Na_2CO_3 (0.213 g), KCl (0.113 g), $K_2HPO_4{\cdot}3H_2O$ (0.115 g), $MgCl_2{\cdot}6H_2O$ (0.155 g), HEPES (8.946 g), NaOH (0.4 g), $CaCl_2$ (0.147g) and Na_2SO_4 (0.036 g) per 500 mL of DIW. The pH of the mSBF was adjusted to 7.4 using NaOH, and the solution was stored at 4 °C before use.

The obtained hydrogels were initially immersed in PBS at 4 °C for 24 hours to remove unreacted monomers, and then the bottom layers of the hydrogels were immersed in the Ca/P metastable solution at room temperature for 3 hours. The hydrogels were then removed, washed with PBS, and soaked in mSBF solution at 37 °C for 32 hours with the exchange of fresh mSBF every 16 hours. The mineralized hydrogels were rinsed with DIW, cut to the required sizes, and stored at 4 °C before use.

Physicochemical characterization of the hydrogel

Cylindrical hydrogels with both a diameter and height of 8 mm were lyophilized and cut for scanning electron microscopy (SEM; Nova NanoSEM 450, FEI, USA) observation. X-Ray diffraction (XRD; Ultima IV, Rigaku, Japan) patterns were also detected for the hydrogels after mineralization. Meanwhile, the dried hydrogels were weighed and marked as W_0. They were then immersed in DIW at 37 °C. After 24 hours, the hydrogels were taken out and weighed again, marked as W_1. The swelling ratio (SR) of the hydrogel was calculated as

$$SR = (W_1 - W_0)/W_0 \quad (2)$$

Hydrogels of the same size as for SEM observation were also tested for their mechanical properties using a universal testing machine (HZ-1004, Hengzhun, China). A compressive rate of 0.2 mm min^{-1} was applied, and the test was terminated once the hydrogel had fractured. Stress–strain curves were obtained and utilized for calculation of the compressive modulus value (normally ~0–3% strain).

The rheological properties of the hydrogels were characterized at room temperature using an Anton Paar rheometer (MCR 302, Austria). Samples with a diameter of 25 mm and a thickness of 2 mm were placed between the bottom and upper plates of the rheometer. The strain sweep was carried out for the deformation range from 0.1 to 100 at a shear stress of 0.1 N and a frequency of 1 Hz. The frequency sweep was conducted from 0.1 to 100 Hz with a shear deformation of 1%.

In vitro cell culture

Isolation and evaluation of BMSCs. Single-layer hydrogel sheets (10 mm in diameter and 1 mm in thickness or 20 mm in diameter and 1 mm in thickness) were prepared in the same manner as for the bilayer hydrogels as described in the 'Preparation of bilayer hydrogel' section. The formula of each group is listed in Table S1 (ESI†). All the hydrogels were first immersed in DIW for 24 hours to remove impurities, sterilized in 75% alcohol solution for 1 day and then immersed in PBS for another day. After that, the hydrogels were exposed to UV light for at least 3 hours and placed at the bottom of a 24-well culture plate.

BMSCs were isolated from new-born Sprague Dawley (SD) rats (1 week). In brief, bone marrow was collected and cultured in a medium of 90% α-MEM, 10% fetal bovine serum (FBS) and 1% penicillin streptomycin under a 5% CO_2 atmosphere at 37 °C. BMSCs were sub-cultured and harvested at passage 3 for the following experiments.

BMSCs were seeded in a 24-well culture plate on the surfaces of bottom layer hydrogels (10 mm in diameter and 1 mm in thickness) at a density of 20 000 cells per well. The plates were incubated under 5% CO_2 at 37 °C with the culture medium changed every other day. After 3 days of incubation, fluorescence microscopy (Olympus FV1000) was utilized to observe the attachment of the cells. To visualize the adhesion of the cells on the hydrogel, the nuclei of the BMSCs were stained with DAPI, while the F-actin of the cells was stained with rhodamine phalloidin.

Differentiation of BMSCs. To evaluate the differentiation of the BMSCs, cells were seeded in a 12-well culture plate (20 mm in diameter and 1 mm in thickness) on the surface of bottom-layer hydrogels at a density of 50 000 cells per well and then cultivated in a humidified atmosphere at 37 °C with 5% CO_2. After cultivation for 1 day, the culture medium was changed to an osteogenic induction medium (90% DMEM supplemented with 10% FBS, 100 nM dexamethasone, 10 mM sodium β-glycerophosphate, and 0.05 mM 1-ascorbic acid-2-phosphate) for further incubation for 21 days. After 7, 14 and 21 days of incubation, the cells were washed with PBS 3 times, treated with 3 freeze–thaw cycles, followed by ultrasonication (SCIENTZ-IID, NingboScientz Biotechnology Co., Ltd, China). The obtained lysate was centrifuged at 14 000 rpm for 20 min, and the supernatant was collected for alkaline phosphatase (ALP) activity, the content of total proteins and Col-I measurements. Specifically, the ALP and Col-I results were normalized to the total protein content examined using a BCA protein assay kit.

Real-time polymerase chain reaction (RT-PCR) was performed to evaluate the gene expression of osteogenic differentiation. In brief, the total RNA was extracted using an RNA isolation kit (Vazyme Biotech Co., Ltd), which was further reverse-transcribed into cDNA using a cDNA synthesis kit (Thermo Fisher Scientific, USA). The cDNA solution was mixed with qCR Master Mix (Bio-Rad) to amplify and evaluate the gene expression of Col-I, osteocalcin (OCN) and runt-related transcription factor 2 (Runx2) using the RT-PCR detection system (CFX96TM, Bio-Rad, USA). The gene expression level of each group was normalized to the control group (BMSCs cultured on a blank culture plate). The primer sequences of each gene are illustrated in Table S2 (ESI†).

Isolation and evaluation of chondrocytes

Articular cartilage was obtained from the hip and ankle joints of new-born SD rats (1 week). Chondrocytes were collected by digestion of articular cartilage using collagenase II (0.2 wt%) and cultured in a complete culture medium (containing 90% DMEM/Ham's F-12 medium, 10% FBS and 1% penicillin-streptomycin). Cells were seeded in a 24-well culture plate on

the surfaces of upper-layer hydrogels (10 mm in diameter and 1 mm in thickness) at a density of 20 000 cells per well. The plates were incubated under 5% CO_2 at 37 °C with the change of culture medium every other day. After 3 days of incubation, the morphologies of the cells on the hydrogels were observed using fluorescence microscopy (Olympus FV1000) with the nuclei and F-actin stained by DAPI and rhodamine phalloidin, respectively.

To evaluate the protein secretion and gene expression of chondrocytes, cells were seeded in a 12 well culture plate (20 mm in diameter and 1 mm in thickness) on the surfaces of upper layer hydrogels at a density of 50 000 cells per well and then cultivated in a humidified atmosphere at 37 °C with 5% CO_2. After 7, 14 and 21 days of incubation, chondrocytes were rinsed with PBS, treated with 3 freeze–thaw cycles followed by ultrasonication (SCIENTZ-IID, NingboScientz Biotechnology Co., Ltd, China). The supernatants were collected *via* centrifugation at 14 000 rpm for 20 min, and then examined using a rat Col-II ELISA kit, a rat GAG ELISA kit and a BCA protein assay kit. Notably, the concentrations of Col-II and GAG were normalized using the protein content obtained from the BCA assay kit.

The characterization of the gene expression of the chondrocytes is similar to that of the BMSCs, except that the gene expression of Col- II, AGG and Sox9 was studied. The primer sequences of each gene are illustrated in Table S2 (ESI†).

In vivo evaluation

***In vivo* degradation and biocompatibility.** The animal study was approved by the Animal Ethical Committee of West China Hospital, Sichuan University. All animals were obtained from the Experimental Animals Centre of West China Hospital, Sichuan University. Eighteen female Sprague Dawley (SD) rats (120–140 g, 9 rats for each group) were utilized to assess the biocompatibility and degradation of the bilayer hydrogels. The mineralized bilayer hydrogels (8 mm in diameter and 4 mm in thickness) were prepared and sterilized in 75% alcohol solution for 1 day and then immersed in PBS for another day. After that, the hydrogels were exposed to UV light for at least 3 hours. Rats in each group were anesthetized using pentobarbital sodium (3 wt%, 40 mg kg^{-1}). Afterwards a 10 mm long incision was created on the back of the rats. For the control group, the incision was sutured without implantation, while for the experimental group, the sterilized hydrogel was implanted underneath the skin and the incision was then sutured immediately. Penicillin (160 000 units per rat) was applied after the operation to avoid infection. After 1, 4 and 8 weeks of implantation, the implanted hydrogels were taken out. In the meantime, the subcutaneous tissues at the implantation sites were extracted and ground with normal saline at a concentration of 0.25 g mL^{-1}. The obtained homogenate was centrifuged at 10 000 rpm for 20 min, then the supernatant was examined using ELISA kits to determine the amounts of IL-1β, IL-6 and TNF-α. The extracted skins were also stained with hematoxylin–eosin (H&E) to evaluate the biocompatibility. Histopathological analysis was carried out and blindly scored as reported in the literature.[26] In brief, scores of 0 and 1 represent no inflammatory cells and a few scattered inflammatory cells, respectively. The score of 2 denotes distinct inflammatory infiltrates around blood vessels, while that of 3 stands for extensive perivascular cuffing with extension into adjacent parenchyma.

***In vivo* knee joint repair.** Twenty New Zealand white rabbits (2.5–3 kg) were separated into four groups randomly. The upper layer, the mineralized bottom layer and mineralized bilayer hydrogels with a diameter of 5 mm and a thickness of 4 mm were prepared and sterilized as described before. The operation was carried out under sterilized conditions. The rabbits were first anesthetized with pentobarbital sodium (3 wt%, 40 mg kg^{-1}). Osteochondral defects with a diameter of 5 mm and thickness of 4 mm were fabricated through the articular and subchondral bone layers of the patellar grooves in both legs of the rabbits using a drill. The defects of the three experimental groups were treated using upper layer, mineralized bottom layer and mineralized bilayer hydrogels, respectively, while the control group was treated with nothing. The wound was sutured and sterilized with povidone-iodine. The rabbits were injected with penicillin (80 units per mL) to avoid infection in the following three days after surgery. The knee joints of each rabbit were collected at 6 weeks after operation and photographed using an optical camera for gross observation. Afterwards the samples were fixed in 10% formalin, and evaluated using a micro-CT scanner (μCT 50, Scanco, Switzerland). The set parameters were as follows: voxel size of 15 μm in all three axes and 380 slices contained in the region of interest (ROI). Three-dimensional reconstructions were performed using a threshold of 200 ranging from 200–1000, as referred to in the literature.[27] After observation samples were decalcified and embedded with paraffin for histological evaluation *via* H&E and safranin O-fast green staining. Immunohistochemical stains including Col-I and Col-II were also applied to assess the regeneration of cartilage and the subchondral bone defect.

Statistical analysis

The results were obtained as the mean and standard deviation of at least three duplicate samples. The GraphPad Prism 6.0 software was used for statistical analysis. A two-tailed Student's *t*-test was applied to compare the statistics between the two groups, and one-way ANOVA was applied for multiple comparisons; $p < 0.05$ was regarded as statistically significant. The indicators *, **, and *** denote $p < 0.05$, $p < 0.01$, and $p < 0.001$, respectively.

Results and discussion

Characterization of synthesized molecules

GelMA was synthesized by the methacrylation of the amine groups of gelatin under mild conditions (Fig. 1a).[22] Gelatin and GelMA were dissolved in D_2O for ^1H NMR measurements. As shown in Fig. 1b, the spectrum of gelatin shows the characteristic methyl or methylene resonances of the amino acids: leucine, valine and isoleucine at 0.87 ppm, threonine at 1.16

ppm, alanine at 1.35 ppm, lysine at 1.61/2.93 ppm, arginine at 1.74/3.16 ppm, aspartic acid at 2.66 ppm and proline at 3.58 ppm.[28] After methacrylation, the typical peaks at δ = 5.38 and 5.64 ppm newly appeared, accompanied by the increase of the methyl group signal at δ = 1.86 ppm, which are assignable to the acrylic protons of methacrylate groups. In addition, the signal of lysine (δ = 2.93 ppm) decreases. This result is in good accordance with the previous study,[29] which confirms the successful methacrylation of gelatin. The DS of the obtained GelMA was estimated *via* the OPA method and was calculated to be 87.5%, suitable for further use.[30]

The synthesis of AGA is completed by the reaction of AG with acryloyl chloride (Fig. 1c).[31] The ^{1}H NMR spectrum of AGA (D_2O) exhibits distinct peaks at $\delta \approx$ 6.10–6.30 ppm and $\delta \approx$ 5.68–5.74 ppm compared with that of GA (Fig. 1d), which are derived from the vinyl protons of acrylate groups. The other peaks are in good accordance with those reported in the literature: δ(ppm): 6.09–6.31 (H_h, H_i, *anti*), 5.68–5.74 (H_i, *syn*), 5.13–5.14 (H_a) and 4.66–4.67 (H_a), 3.35–3.91 (H_b, H_c, H_d, H_e, and H_f).[32] The mass spectrum of AGA further reveals an intense peak at m/z 256.07 (calculated AGA + Na^+: 256.08), which accounts for the acylation of the amino group (Fig. 1e). The ^{1}H NMR results together with the mass spectrum confirm the existence of the acrylate group on the AGA molecule.

Fundamental properties of the hydrogels

To mimic the natural ECM of cartilage, AGA as the abundant glycosaminoglycan rich in cartilage was incorporated with GelMA to form the upper-layer scaffold. The ratio of GelMA and AGA was regulated to investigate their influence on the mechanical properties. As shown in Fig. 1f and g, the compressive modulus of the hydrogel increases from 11.22 kPa (G9A1) to 131.5 kPa (G19A1) when the content of GelMA is increased. It has been acknowledged that the stiffness of the scaffold plays a crucial role in the differentiation of stem cells.[33,34] For the bone marrow mesenchymal stem cells, the favourable stiffness for their differentiation into chondrocytes is about 80 kPa, while that for osteoblasts is 110–190 kPa.[16,35] It is notable that the mechanical property of the G14A1 group (80.99 kPa) meets the requirements for chondrogenic differentiation. In this sense, the ratio of GelMA to AGA was fixed at 14 : 1 for the following experiments.

Meanwhile, VPA was co-polymerized with AAm to act as the bottom-layer scaffold for calcified cartilage. These two layers were sutured together with the assistance of alginate–calcium chelation (see the details in the Experimental section). The direct addition of the precursor solution of the upper hydrogel to that of the bottom hydrogel destroyed the intrinsic integrity of the two separate layers. As a consequence, the precursor solution of the bottom-layer hydrogel was pre-cured using UV irradiation first, followed by the pouring of the upper precursor solution and further UV curing. A pre-curing time of 3, 5 and 7 min was applied to investigate the interfacial bonding between the two layers. The rheological properties of the as-obtained double-layer hydrogels were characterized by subjecting each sample to shear stress. The oscillatory strain sweeps reveal that the storage modulus (G') maintains its stability and

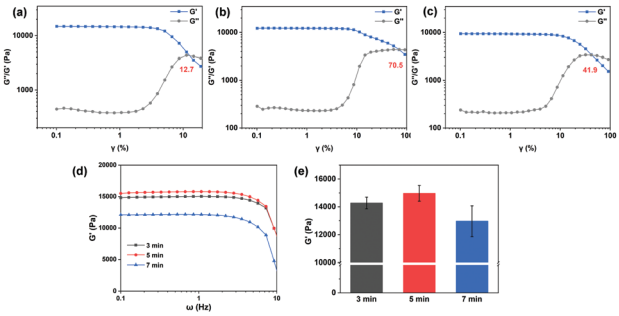

Fig. 2 Shear strain-dependent storage modulus (G') and loss modulus (G'') of the double-layer hydrogel when the bottom layer was pre-cured for (a) 3 min, (b) 5 min and (c) 7 min; (d) storage moduli of the above hydrogels as a function of frequency (ω); and (e) static moduli of hydrogels collected at a frequency of 1 Hz and 25 °C.

is higher than the loss modulus (G'') at a low deformation strain, indicating gel-like behaviour under these conditions (Fig. 2a–c).[36] When the shear strain was increased above a critical value, G' decreased to lower than G'' and the gel state of the hydrogel was disrupted. For hydrogels with pre-curing times of 3, 5 and 7 min, the critical strains are 12.7%, 70.5% and 41.9%, respectively. These results reveal that the irradiation time of 5 min enables the largest resistance to shear deformation. Moreover, the frequency sweeps for each group were recorded (Fig. S1, ESI†). The linear viscoelastic region of G' at low frequency ($\sim$0.1–5 Hz) denotes the stable mechanical performance of the hydrogel over the long-term (Fig. 2d).[37] It should be mentioned that the modulus of the double-layer hydrogel shows a slight increment (14.28 to 14.97 kPa) when the pre-curing time is prolonged from 3 to 5 min, and shows a sharp decrease (12.97 kPa) with the pre-curing time of 7 min (Fig. 2e). It is speculated that the compositions of the upper and bottom layers might interfere with each other under too short a pre-curing time (3 min). On the contrary, excessive pre-curing (7 min) is disadvantageous for efficient interfacial bonding since the inter-diffusion and chelation around the interface are largely weakened. Consequently, a pre-curing time of 5 min generates the best mechanical performance of the double-layer hydrogel, which is optimized for the following experiments.

The chelation between sodium alginate and calcium ions is beneficial for the interfacial bonding between the two layers. As shown in Fig. 3, the double-layer hydrogel without chelation could resist the shear deformation of only 16.1%, much lower than that of the chelated double-layer hydrogel (70.5%, Fig. 2b). The distinct discrepancy between pure upper- or bottom-layer hydrogels (critical deformation higher than 50%) reveals that the disruption originates from the interface. Meanwhile, the modulus of the double-layer hydrogel (13.68 kPa; Fig. S2 (ESI†) and Fig. 3d and e) is lower in comparison with that of the hydrogel with chelation (14.97 kPa, Fig. 2e). In addition, the interfacial bonding is still maintained to a certain extent after mineralization, considering that the mineralized double-layer hydrogel has a critical deformation strain of 56.1% (Fig. 3d) and a G' value of 19.21 kPa (Fig. 3e and f).

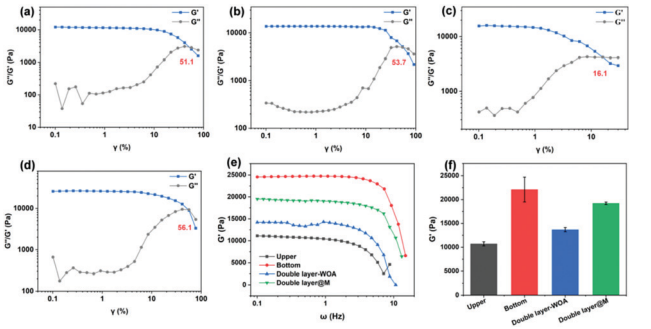

Fig. 3 Shear strain-dependent storage modulus (G') and loss modulus (G'') of (a) upper, (b) bottom, and (c) double-layer hydrogels without chelation, and (d) the double-layer hydrogel after mineralization; (e) storage moduli of the above hydrogels as a function of frequency (ω); and (f) static moduli of hydrogels collected at a frequency of 1 Hz and 25 °C.

The as-prepared bilayer hydrogel shows an opaque white appearance in the upper layer and a transparent appearance in the bottom layer. This non-uniform hydrogel becomes wholly opaque after lyophilization (Fig. S3a, ESI†). The swelling ratio of the hydrogels was examined by immersion in deionized water (Fig. S3b, ESI†). The bottom layer exhibits a higher swelling ratio (approximately 650%) than that of the upper layer (approximately 470%), and the swelling ratio of the bilayer hydrogel lies in between (about 540%). The excellent swelling behavior of the hydrogels is probably due to the hydrophilic groups such as amine, amide, hydroxyl and phosphate in each layer. The affinity of AAm, VPA and alginate for water is regarded as being higher than those of GelMA and AGA,[38,39] which generates a higher swelling ratio for the bottom layer. To clarify this heterogenous property of the bilayer hydrogel, SEM was adopted to characterize the interior structure of the hydrogel. As shown in Fig. 4a, a clear boundary between the upper and bottom layers can clearly be recognized from the SEM image. The upper layer possesses large pores with an average size of 217 μm (Fig. 4d), while the bottom layer exhibits interconnected smaller pores (82 μm on average) (Fig. 4e). After mineralization, a significant swelling behavior can be visualized in the bottom layer as the size of the pores increases to about 112 μm (Fig. 4f). The statistical pore size of each layer is summarized in Fig. 4g, h and i, which confirms the heterogenous architecture of the bilayer hydrogel. Generally, large interconnected porosity is advantageous for cell infiltration, mass transport and vascularization.[40] A macroporous hydrogel (a pore size above 10 μm) with a high pore size is thus usually sought.[41] As reported in previous studies, larger pore sizes could drastically improve chondrogenesis, whereas the subchondral phase favours smaller pore sizes.[4] Although a consensus has not been reached for the specific pore size for chondrogenic or osteogenic differentiation in various studies,[42–44] the pore size of 100 μm is reported to be beneficial for vascularisation and bone ingrowth.[45] In this regard, it is anticipated that the pore size of the hydrogel in our experiments could meet the requirements for bio-functionality.

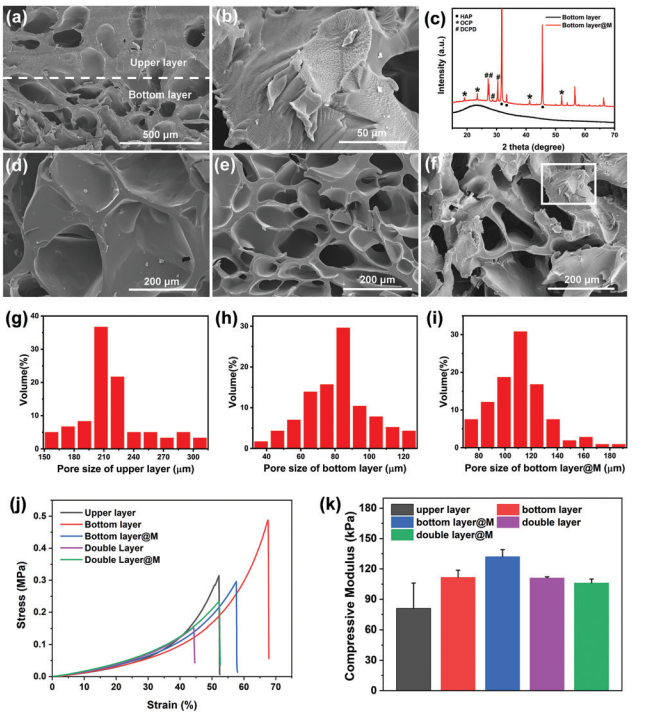

Fig. 4 (a) SEM image of the interfacial structure of the bilayer hydrogel. (b) Magnification of (f). (c) XRD patterns of the bottom-layer hydrogel before and after mineralization. (d) and (e) Enlarged views of the upper-layer and bottom-layer areas, respectively. (f) SEM image of mineralized hydrogel. (g), (h) and (i) Pore size distributions of different sections of hydrogel analyzed using SEM images. (j) Compressive strain–stress curves and (k) compressive moduli of different hydrogels.

In addition, the pore size of the hydrogel is closely associated with the mechanical properties of the hydrogel, where, usually, the stiffness of the scaffold decreases as the porosity increases.[46] For a higher stiffness of the bone layer in our experiments, smaller pore size is sought. It should be mentioned that the pores are interconnected with each other, as shown by the reconstructed micro-CT images of the double layer hydrogel (Fig. S4, ESI†) and SEM images of the hydrogel at different sites (Fig. S5, ESI†). To summarize, the mineralized bilayer hydrogel maintains a pore size of 100–300 μm, which is suitable for cell infiltration and vascularization.

For the hydrogel after mineralization, a thin layer of minerals was deposited on the surface of the polymeric network, even on that of the inner hydrogel (Fig. 4b), suggesting an in-depth mineralization process. Compared with the broad peak of an amorphous hydrogel without mineralization, the XRD pattern of a mineralized hydrogel shows intense sharp peaks, further confirming the existence of crystalline minerals (Fig. 4c). The diffraction peaks at $2\theta = 31.6^\circ$ and $2\theta = 33.4^\circ$ correspond to the (211) and (300) planes of hydroxyapatite (HAP). The strong diffraction peak at $2\theta = 44.5^\circ$ is possibly attributed to the (203) plane. Besides, other crystalline forms of calcium phosphate, such as dicalcium phosphate dihydrate (DCPD) and octacalcium phosphate (OCP), are also detected.

In order to reveal the effect of minerals on the mechanical properties of the hydrogel, the compressive stress–strain curves

for hydrogels of different groups were measured (Fig. 4j), and the compressive modulus values calculated from the curves are listed in Fig. 4k. The upper layer exhibits a relatively soft and brittle property with a modulus of 81 ± 25 kPa and a stain of less than 55%. In comparison, the bottom layer possesses an enhanced modulus (112 ± 7 kPa) and a larger strain (68%), while the bilayer hydrogel shows an intermediate modulus (111 ± 12 kPa). After mineralization, the modulus of the bottom layer further improves to 132 ± 7 kPa with a decrease in the strain (58%), suggesting that the mineralization strengthens the modulus and stiffness of the hydrogel. Interestingly, for the mineralized bilayer hydrogel, its modulus decreases slightly to 106 ± 4 kPa, which might be explained by the weakening of the chelation between calcium ions in the upper layer and alginate in the bottom layer caused by mineralization (as confirmed by the rheological properties of the hydrogel before and after mineralization in Fig. 2 and 3). The mechanical properties of the hydrogel alter from the upper to the bottom layer, and satisfy the needs for chondrogenic and osteogenic differentiation of stem cells, respectively.[16,35] Overall, the mineralized bilayer hydrogel has a suitable pore size, mechanical properties and, more importantly, a matched chemical composition with the ECM of natural osteochondral cells, so its biochemical properties are explored in the following.

In vitro cell assessment of bottom-layer hydrogel using BMSCs

BMSCs were seeded on the bottom-layer hydrogel to evaluate the cell behavior. Here, bare polyacrylamide (pAAm) and polyacrylamide–vinylphosphonic acid copolymer hydrogels before (pAAm–VPA) and after mineralization (pAAm–VPA@M) were compared (Table S1, ESI†). The cell affinity of the hydrogels was initially visualized using fluorescence microscopy after cultivation for 3 days (Fig. 5a–f). For the pAAm group, the cells were distributed sporadically on the surface. By contrast, uniformly distributed cells were discovered in the pAAm–VPA and pAAm–VPA@M groups. Note that the cells spread well on the pAAm–VPA@M hydrogel, and the cytoskeleton (the red colour in Fig. 5) was more stretched out than those on pAAm and pAAm–VPA, which implies the positive role of minerals in the adhesion of BMSCs.

Osteogenic differentiation is a cell-mediated process, during which some osteogenic-related genes are activated, and the secreted proteins are promoted. Here, the osteogenic differentiation of BMSCs was assessed on the bottom-layer hydrogel. The key osteogenic markers, Col-I and ALP activities, were detected after cultivation for 7, 14 and 21 days.[47] The secretion of Col-I and ALP activities increased continuously with the passage of time (Fig. 5g and h). Compared with the pAAm and pAAm-VPA groups, the production of Col-I and ALP by the pAAm-VPA@M group is significantly enhanced. In particular, after 14 days of incubation, compared with pure pAAm (171 U per g protein) and pAAm-VPA (224 U per g protein), the pAAm-VPA@M group (838 U per g protein) exhibits ALP activity that is 3.7-fold higher. As the incubation time was extended to 21 days, the ALP secretion in all three groups

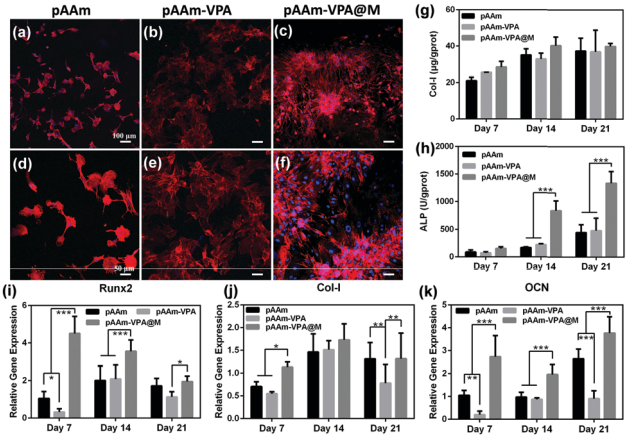

Fig. 5 *In vitro* analysis of bottom-layer hydrogels. (a–c) Fluorescence microscopy images of BMSCs cultured on bottom-layer hydrogels for 3 days, and (d–f) enlarged images of (a–c) (red, cytoskeletons; blue, nuclei; and scale bars, 100 μm and 50 μm). Amounts of (g) Col-I and (h) ALP levels after cultivation for 7, 14 and 21 days. The expression of osteogenic-related (i) Runx-2, (j) Col-I, and (k) OCN genes after incubation for 7, 14 and 21 days. Significances ($p < 0.5$, $p < 0.01$ and $p < 0.001$) are denoted by the asterisks (*, ** and ***), respectively.

increased and the superiority of the pAAm-VPA@M group was maintained.

Thereafter, the expression of osteogenic differentiation-related genes, Runx2, Col-I and OCN was monitored using the pure culture plate as a reference. As shown in Fig. 5i–k, generally, pAAm-VPA@M apparently elevated Runx2, Col-I and OCN gene expression over 21 days of culture in comparison with pAAm and pAAm-VPA. In detail, the expression of Runx2 was the highest on day 7 and then declined afterwards. By contrast, Col-I and OCN displayed growing expressions from 7 to 21 days. The expression of these genes accords well with the rhythm of osteogenic differentiation.[48] As for the pAAm and pAAm-VPA groups, the introduction of VPA had an adverse effect on osteogenic differentiation, given that the expressions of Runx2, Col-I and OCN were attenuated to some extent. All these results confirm that pAAm-VPA@M is suitable as a scaffold for the repair of sub-cartilage bone, in consideration of its excellent osteogenic differentiation ability.

In vitro cell assessment of upper-layer hydrogel using chondrocytes

Similarly, chondrocytes were seeded on the upper-layer hydrogel for cell evaluation. In an attempt to clarify the effect of GelMA and AGA, pure poly(ethylene glycol) diacrylate (PEGDA), and GelMA and GelMA–AGA copolymer hydrogels were prepared for comparison (Table S1, ESI†). Fig. 6a–f show the fluorescence images of chondrocytes on the hydrogel surface after cultivation for 3 days. For all the groups, the surface of the hydrogel was almost fully covered by chondrocytes, indicating a good adhesion ability. It is noteworthy that the chondrocytes maintained a rounded cellular morphology after 7 days and cell aggregates were distinctively observed, implying the chondrocytic phenotype on the hydrogels[49] (Fig. S6, ESI†).

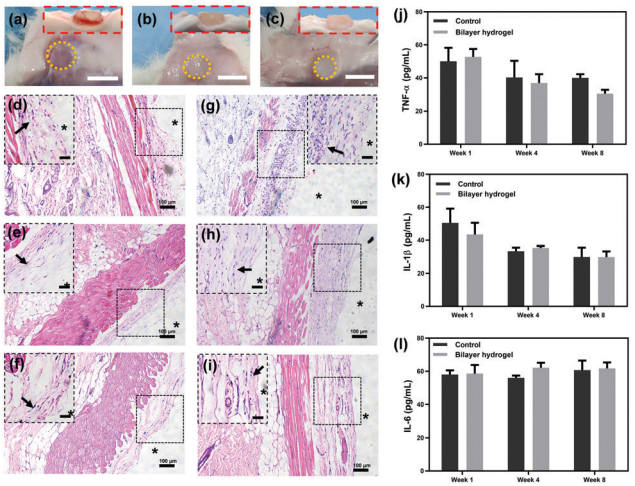

Fig. 6 *In vitro* analysis of upper-layer hydrogels. (a–c) Fluorescence microscopy images of chondrocytes cultured on upper-layer hydrogels for 3 days, and (d–f) enlarged images of (a–c) (red, cytoskeletons; blue, nuclei; and scale bars, 50 μm and 25 μm). Amounts of (g) Col-II and (h) GAGs levels after cultivation for 7, 14 and 21 days. The expression of chondrogenesis-related genes (i) Col-II, (j) Sox9, and (k) AGG after incubation for 7, 14 and 21 days. Significances ($p < 0.5$, $p < 0.01$ and $p < 0.001$) are suggested by the asterisks (*, ** and ***), respectively.

Next, to investigate the effect of the hydrogel on chondrogenic differentiation, the cell activity of the chondrocytes was evaluated by measuring the protein synthesis on the upper-layer hydrogel. As the main components of the cartilage extracellular matrix (ECM),[50] the Col-II and GAGs levels were detected *via* ELISA kit at set time intervals (Fig. 6g and h). The contents of Col-II for all three groups showed not much difference on Day 7, and ascended slowly during further incubation. Chondrocytes on the GelMA–AGA surface produced remarkably higher levels of Col-II than the other two groups on Day 14 and Day 21. In addition, the secretion of another essential chondrogenic component, GAGs, is closely related to AGA. No significant differences are observed for the concentration of GAGs on PEGDA and GelMA, while GAGs on GelMA–AGA showed an apparent increase in comparison. The secretion of Col-II and GAGs together confirms that AGA in the hydrogel facilitates the chondrogenic activity.

Meanwhile, the gene expressions of chondrogenic markers, Col-II, SOX9 and AGG, were assessed to predict the trend of chondrogenesis by the hydrogels (Fig. 6i–k).[51] The gene expressions of Col-II and SOX9 for the GelMA–AGA group were the highest among the three groups on Day 7 and Day 21. Similarly, the AGG expression on GelMA–AGA was superior to that on PEGDA and GelMA over the whole incubation, and was significantly higher on Day 21 (Fig. 6k). By contrast, the expressions of chondrogenic markers for the PEGDA and GelMA groups were lower and approximately equal with each other. Based on the above results, AGA is beneficial for chondrogenic differentiation, while the effect of GelMA is not comparable. Therefore in the following experiments, GelMA–AGA was chosen for fabrication of the upper-layer scaffold.

In vivo evaluation

***In vivo* degradation and compatibility assessment.** In view of the above cell experiments, the bilayer hydrogel constituted of pAAm–VPA@M (bottom layer) and GelMA–AGA (upper layer) was fabricated. *In vivo* degradation and compatibility of the bilayer hydrogel were assessed by subcutaneous implantation into SD rats. The body weights of the rats were recorded periodically after subcutaneous implantation to evaluate the health condition of the animals. As shown in Fig. S7 (ESI†), the rats showed rapid body weight growth (*ca.* 40 g per week) in the first two/three weeks post-surgery for the experimental and control groups, respectively. After that, the weights increased slowly (*ca.* 9.7 g per week) until the end of 8 weeks. During the whole period, the average body weight of the hydrogel group was slightly lower than that of the control group, and the growth patterns of both groups were very close. This means that the activities of the SD rats are not affected by the implantation of hydrogels.

The appearance of the hydrogels was observed after 1, 4 and 8 weeks of implantation. The yellow dotted circles in Fig. 7a–c illustrate the outlines of the hydrogels. The areas of the hydrogels exhibited a tendency for reduction and the weight of the hydrogels also decreased (Fig. S8, ESI†), which is ascribed to their slow degradation *in vivo*. Even so, it might take more time for complete degradation, considering the fact that the hydrogels still exist after 8 weeks. To evaluate the inflammation, the subcutaneous tissue around the hydrogel was observed. As illustrated in the inset of Fig. 7a, the tissue wrapping the hydrogels was red and inflamed from the examination after one week, which can also be seen from the surrounding tissue fluid in the side view. However, the inflammation response subsided after 4 weeks (Fig. 7b). Furthermore, near-normal

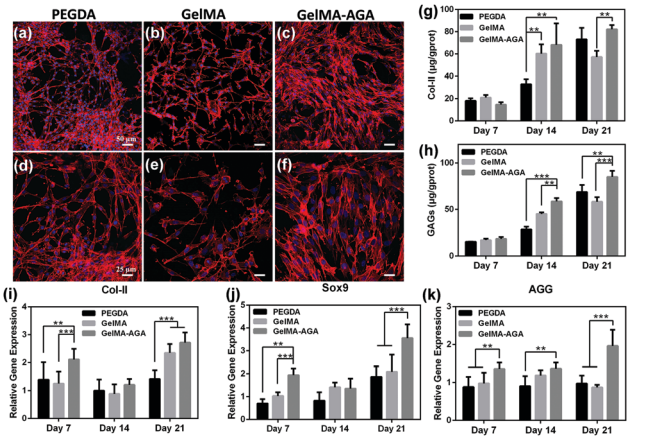

Fig. 7 *In vivo* inflammation observation of hydrogels ($n = 3$). Photographs of hydrogels and the surrounding tissues at (a) 1, (b) 4 and (c) 8 weeks post-surgery. Scale bar, 1 cm. The insets show the side views. H&E stains of subcutaneous tissue in the (d–f) control and (g–i) hydrogel groups after 1, 4 and 8 weeks. The insets show the enlarged areas adjacent to the hydrogels. Scale bar, 50 μm. The '*' symbols represent the hydrogels, and the black arrows indicate macrophages. The levels of (j) tumor necrosis factor-α, (k) interleukin-1β and (l) interleukin-6 for the control and bilayer hydrogel groups, respectively.

subcutaneous tissue with no inflammation was observed after 8 weeks (Fig. 7c), and the hydrogel was well integrated with the surrounding tissues (inset in Fig. 7c).

H&E staining was then applied to further analyse the inflammation of the subcutaneous tissues. As shown in Fig. 7d and g, a massive accumulation of macrophages (indicated by the black arrows in Fig. 7d and g) in both groups represents the acute inflammatory reaction during the early period (one week). This situation changed after 4 weeks of implantation. Significantly reduced inflammatory cells were observed, although some still remained in the subcutaneous fascia and muscles (Fig. 7e and h). After 8 weeks, an attenuated inflammatory response was detected, given that only sporadic inflammatory cells could be found (Fig. 7f and i). The inflammation of the hydrogel group does not show any significant differences with the control groups during the whole period. Tissue inflammation was also blindly scored for better illustration.[26] As shown in Fig. S9 (ESI†), the scores of both groups were about 3 after one week, which meant obvious inflammation. After 4 weeks, the scores declined to about 2, suggesting inflammation relief in small areas. After 8 weeks, the scores further reduced to about 1, showing signs of mild inflammation. There is no significant difference between the control and the hydrogel groups. The decline of the inflammatory response for the hydrogel group might be originating from the degradation of the hydrogel, considering that a sustained inflammatory response could occur for the implantation of non-degradable materials.[52]

In addition, the inflammatory response markers TNF-α, IL-1β and IL-6 were quantitatively measured to evaluate the tissue inflammation.[53,54] TNF-α is an important cellular inflammatory factor, which is mainly produced by monocytes. As shown in Fig. 7j, both groups produced considerable TNF-α (about 51 pg mL^{-1}) after 1 week of implantation, suggesting that acute inflammation occurred. The concentration of TNF-α in the hydrogel group was slightly higher than that of the control group. After 4 and 8 weeks, the secretion of TNF-α in both groups constantly decreased, while the TNF-α level of the hydrogel group gradually fell below that of the control group. No significant differences are observed for both groups during the whole of the 8 weeks. This phenomenon indicates the good biocompatibility of the hydrogel.

Interleukins (ILs) are an essential category of cytokines, among which IL-1β and IL-6 play a significant role in the immune regulation and inflammatory response processes.[55,56] The pattern of IL-1β secretion is illustrated in Fig. 7k. Similar to the tendency of TNF-α, both the groups exhibited high levels of IL-1β in the early stage. The amount of IL-1β drastically decreased after 4 weeks, and remained almost the same after 8 weeks without any significant difference between the two groups. This result confirms the existence of acute inflammation during the early period. After that, the inflammation response gradually subsided and finally reached a plateau. Another cytokine, IL-6, secreted by T cells and macrophages, stimulates the immune response and resists infection.[57,58] Both groups showed no obvious changes in IL-6 during the whole process (Fig. 7l), which indicates the sustained anti-inflammation response. In brief, there were no significant differences between the control and experimental groups with respect to the three markers, proving the acceptable compatibility of the bilayer hydrogel with subcutaneous tissues.

Articular implantation evaluation

To test the ability of the bilayer hydrogel to repair osteochondral defects *in vivo*, defects (5 mm in diameter and 4 mm in depth) on the knee joints of rabbits were first developed, and hydrogels were then placed in the osteochondral defects for evaluation. The whole process was photographed and is shown in Fig. 8a. Four groups were compared in this experiment: the defects of the control group were left without any treatment, while those of the other groups were treated by upper-layer, bottom-layer and bilayer hydrogels correspondingly. The knee joint samples were collected after 6 weeks of implantation. As shown in Fig. 8b, the bilayer group has the best regeneration without any obvious border with the surrounding tissue, however, the other groups all exhibited clear defects with distinct boundaries. The International Cartilage Repair Society (ICRS) macroscopic score method[59] was utilized to analyse the samples. As shown in Fig. 8c, the score of the bilayer group is the highest among all the groups and the difference was considered to be significant ($*p < 0.05$). Besides, the score of as high as 8 means that the regenerated tissue is the closest to normal tissue.

Micro-CT is utilized to analyse the content of bone minerals in our experiments. As illustrated in Fig. S10a (ESI†), the tissue surrounding the hydrogel in all 4 groups was initially regenerated to different extents, especially the superficial area. The superficial defects of the bilayer group exhibited better

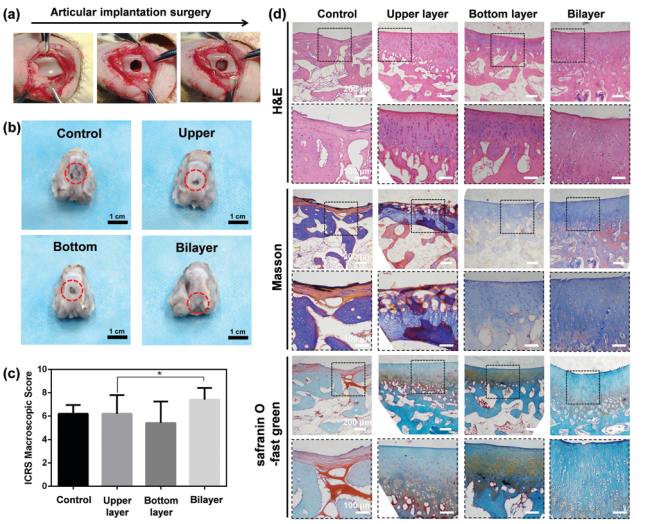

Fig. 8 (a) The process of articular implantation surgery. (b) Macroscopic observation of knee joints and (c) ICRS macroscopic scores (n = 5) for different groups after 6 weeks. Significance ($p < 0.5$) is suggested by the asterisk (*). (d) H&E, Masson and safranin O stains of the collected knee joints after 6 weeks of implantation. The black boxes indicate the enlarged areas (scale bars, 200 μm and 100 μm).

regeneration compared with those of the other groups. A volume of interest (VOI) was established for each group for comparison (Fig. S10b, ESI†). The ratio of the bone volume fraction to the total volume (BV/TV), and the bone mineral density (BMD) of the bone volume fraction and of the total volume were calculated from micro-CT results. As shown in Fig. S10c–e (ESI†), all three parameters measured in the bilayer groups were higher than those in the other groups, although the advantage was not significant.

To thoroughly evaluate the repair ability of the different hydrogels, the collected osteochondral samples were sectioned and stained for histological analysis. As shown in Fig. 8d, the typical layered structure of cartilage to bone was not observed in the control group, although an irregular arrangement of cells in the superficial area and a loose fibrous structure in the middle of the defect were visualized. By contrast, newly formed tissues displayed the characteristic layered structure in the three hydrogel groups. In the upper-layer group, the regenerated cartilage tissues exhibited a fibrocartilage-like appearance, as evidenced by an intense Masson staining of Col-I in the upper region (Fig. 8d and Fig. S11, ESI†).[60] In both the bottom-layer and bilayer groups, the arrangement of cells exhibited a slight trend of being parallel with the surface in the superficial area, whilst being vertical to the surface in the deeper zone, similar to that of natural articular cartilage. The expression of Col-I and Col-II was mainly located in the subchondral and articular areas, respectively (Fig. S11 and S12, ESI†). This phenomenon is similar to the distribution in natural tissue.[61] It is noteworthy that the bilayer group induced a thicker regeneration of articular tissue. Apart from that, the formation of new bone in the subchondral zone was distinctly detected for the bottom-layer hydrogel. All these results confirm that the bilayer hydrogel regenerates more intact structures of the defect area, and is advantageous for osteochondral tissue engineering.

We have to admit that although preliminary regeneration has been achieved, this work still has some limitations. Rabbits have a high regenerative ability and different skeletal structures from those of human beings. Hence, large trials should be devoted to confirming the regeneration ability in a real human body environment. Besides, the mechanical properties of the bottom-layer hydrogel could also be improved by the introduction of another network or more inorganic components. Furthermore, the immunomodulatory effects for osteochondral repair will be considered in our further studies.[62,63]

Conclusions

In summary, inspired by the composition of the natural ECM, a heterogenous bilayer hydrogel was constructed for the repair of osteochondral defects. Aiming at cartilage repair, GelMA together with AGA was modified and utilized as the polymer matrix of the upper layer. Meanwhile, acidic groups (VPA) were incorporated into the bottom layer to induce *in situ* biomineralization of CaP, similar to the function of NCPs. The two layers were sutured by inter-diffusion and the chelation of calcium ions and alginate added to the upper and bottom layers, respectively. The obtained hydrogel scaffold shows heterogenous compositions, porosities and mechanical properties. When cocultured with chondrocytes and BMSCs, respectively, both layers show the capability for cell adhesion. More importantly, AGA in the upper layer stimulates the extracellular matrix secretion of chondrocytes (Col-II and GAGs) and the expression of chondrogenesis-related genes. In addition, the minerals inside the hydrogel skeleton enhance the stiffness of the hydrogel and promote the osteogenesis of BMSCs. *In vivo* evaluation of the hydrogel further confirms the feasibility of the hydrogel scaffold. Subcutaneous implantation demonstrates that the hydrogel cannot induce intense inflammation and that the subtle inflammation gradually decreases to a normal level. The subsequent articular cartilage implantation confirms that the bilayer group shows the best repair ability among all the groups. We envision that this cell-free, cost-effective and efficient hydrogel could be potentially applied in a clinical setting for osteochondral repair. The strategy developed here inspires the design of other materials for tissue engineering.

Author contributions

Zhuoxin Chen: investigation, and writing – original draft. Hong Xiao: funding acquisition. Hongbo Zhang: visualization. Qiangwei Xin: investigation. Haochen Zhang: investigation. Haixin Liu: methodology. Qiang Guo: resources. Mingzhen Wu: methodology. Liangrui Zuo: investigation. Jun Luo: validation. Chunmei Ding: conceptualization, and writing – review and editing. Hong Tan: project administration. Jianshu Li: supervision.

Conflicts of interest

There are no conflicts to declare.

Acknowledgements

The authors are grateful to Dr Peijie Tan (West China Hospital of Stomatology, Sichuan University) for kind help with the cell experiments. Suggestive discussions with Dr Peng Yu (College of Polymer Science and Engineering, Sichuan University) are sincerely appreciated. Support from the National Natural Science Foundation of China (51925304, 51973133 and 51903175) and the Sichuan Science and Technology Program (2020YJ0024) is also gratefully acknowledged.

Notes and references

1 X. Feng, P. Xu, T. Shen, Y. Zhang, J. Ye and C. Gao, *J. Mater. Chem. B*, 2020, **8**, 391–405.
2 J. Yang, Y. Liu, L. He, Q. Wang, L. Wang, T. Yuan, Y. Xiao, Y. Fan and X. Zhang, *Acta Biomater.*, 2018, **74**, 156–167.

3 D. Gan, Z. Wang, C. Xie, X. Wang, W. Xing, X. Ge, H. Yuan, K. Wang, H. Tan and X. Lu, *Adv. Healthcare Mater.*, 2019, **8**, 1901103.
4 L. Zhou, V. O. Gjvm, J. Malda, M. J. Stoddart, Y. Lai, R. G. Richards, K. K.-W. Ho and L. Qin, *Adv. Healthcare Mater.*, 2020, **9**, 2001008.
5 A.-M. Yousefi, M. E. Hoque, R. G. S. V. Prasad and N. Uth, *J. Biomed. Mater. Res., Part A*, 2015, **103**, 2460–2481.
6 X. Liu, Y. Wei, C. Xuan, L. Liu, C. Lai, M. Chai, Z. Zhang, L. Wang and X. Shi, *Adv. Healthcare Mater.*, 2020, **9**, 2000076.
7 K. Zhang, S. He, S. Yan, G. Li, D. Zhang, L. Cui and J. Yin, *J. Mater. Chem. B*, 2016, **4**, 2628–2645.
8 X. Hu, Y. Wang, Y. Tan, J. Wang, H. Liu, Y. Wang, S. Yang, M. Shi, S. Zhao, Y. Zhang and Q. Yuan, *Adv. Mater.*, 2017, **29**, 1605235.
9 E. Kunisch, A. K. Knauf, E. Hesse, U. Freudenberg, C. Werner, F. Bothe, S. Diederichs and W. Richter, *Biofabrication*, 2018, **11**, 015001.
10 L. Coluccino, P. Stagnaro, M. Vassalli and S. Scaglione, *J. Appl. Biomater. Funct. Mater.*, 2016, **14**, e42–52.
11 J. Zhou, X. Guo, Q. Zheng, Y. Wu, F. Cui and B. Wu, *Colloids Surf., B*, 2017, **152**, 124–132.
12 J. J. Li, D. L. Kaplan and H. Zreiqat, *J. Mater. Chem. B*, 2014, **2**, 7272–7306.
13 N. Huebsch, P. R. Arany, A. S. Mao, D. Shvartsman, O. A. Ali, S. A. Bencherif, J. Rivera-Feliciano and D. J. Mooney, *Nat. Mater.*, 2010, **9**, 518–526.
14 S. P. Nukavarapu and D. L. Dorcemus, *Biotechnol. Adv.*, 2013, **31**, 706–721.
15 C. Ding, Z. Chen and J. Li, *Biomater. Sci.*, 2017, **5**, 1435–1449.
16 S. H. Oh, D. B. An, T. H. Kim and J. H. Lee, *Acta Biomater.*, 2016, **35**, 23–31.
17 F. Gao, Z. Xu, Q. Liang, H. Li, L. Peng, M. Wu, X. Zhao, X. Cui, C. Ruan and W. Liu, *Adv. Sci.*, 2019, 1900867.
18 K. Cheng, Y. Zhu, D. Wang, Y. Li, X. Xu, H. Cai, H. Chu, J. Li and D. Zhang, *Mater. Sci. Eng., C*, 2020, **117**, 111368.
19 Q. Wang, L. Ren, C. Xu, Z. Zhai, J. A. Zhou, Y. Yao, H. Xia and Y. Wang, *J. Appl. Polym. Sci.*, 2013, **128**, 89–96.
20 H. Yao, J. Xue, R. Xie, S. Liu, Y. Wang, W. Song, D.-A. Wang and L. Ren, *J. Mater. Sci.: Mater. Med.*, 2017, **28**, 170.
21 X. Xu, H. Sun, Y. Wang, H. Cai, D. Zhang, H. Tan and J. Li, *Chem. Commun.*, 2020, **56**, 3633–3636.
22 J. W. Nichol, S. T. Koshy, H. Bae, C. M. Hwang, S. Yamanlar and A. Khademhosseini, *Biomaterials*, 2010, **31**, 5536–5544.
23 T. Matsuda and T. Sugawara, *Macromolecules*, 1996, **29**, 5375–5383.
24 F. C. Church, H. E. Swaisgood, D. H. Porter and G. L. Catignani, *J. Dairy Sci.*, 1983, **66**, 1219–1227.
25 Q. Yang, F. Song, X. Zou and L. Liao, *J. Biomater. Sci., Polym. Ed.*, 2017, **28**, 431–443.
26 N. Liu, Q.-c. Kan, X.-j. Zhang, Y.-m. Xv, S. Zhang, G.-X. Zhang and L. Zhu, *Exp. Mol. Pathol.*, 2014, **97**, 470–476.
27 T. J. Levingstone, E. Thompson, A. Matsiko, A. Schepens, J. P. Gleeson and F. J. O'Brien, *Acta Biomater.*, 2016, **32**, 149–160.
28 X. Hu, D. Li, F. Zhou and C. Gao, *Acta Biomater.*, 2011, **7**, 1618–1626.
29 W. T. Brinkman, K. Nagapudi, B. S. Thomas and E. L. Chaikof, *Biomacromolecules*, 2003, **4**, 890–895.
30 A. H. Nguyen, J. McKinney, T. Miller, T. Bongiorno and T. C. McDevitt, *Acta Biomater.*, 2015, **13**, 101–110.
31 S. S. Ting, E. H. Min, P. B. Zetterlund and M. H. Stenzel, *Macromolecules*, 2010, **43**, 5211–5221.
32 J. Bernard, X. Hao, T. P. Davis, C. Barner-Kowollik and M. H. Stenzel, *Biomacromolecules*, 2006, **7**, 232–238.
33 Y.-K. Wang and C. S. Chen, *J. Cell. Mol. Med.*, 2013, **17**, 823–832.
34 M. Zhang, Q. Sun, Y. Liu, Z. Chu, L. Yu, Y. Hou, H. Kang, Q. Wei, W. Zhao, J. P. Spatz, C. Zhao and E. A. Cavalcanti-Adam, *Biomaterials*, 2021, **268**, 120543.
35 J. Liao, T. Tian, S. Shi, X. Xie, Q. Ma, G. Li and Y. Lin, *Bone Res.*, 2017, **5**, 17018.
36 C. Yan and D. J. Pochan, *Chem. Soc. Rev.*, 2010, **39**, 3528–3540.
37 F. Cuomo, M. Cofelice and F. Lopez, *Polymers*, 2019, **11**, 259.
38 B. Işık, *J. Appl. Polym. Sci.*, 2004, **91**, 1289–1293.
39 S. Sagbas and N. Sahiner, *Fuel Process. Technol.*, 2012, **104**, 31–36.
40 K. S. Lim, M. Baptista, S. Moon, T. B. F. Woodfield and J. Rnjak-Kovacina, *Trends Biotechnol.*, 2019, **37**, 1189–1201.
41 S. A. Bencherif, T. M. Braschler and P. Renaud, *J. Periodontal Implant Sci.*, 2013, **43**, 251–261.
42 H. F. Pereira, I. F. Cengiz, F. S. Silva, R. L. Reis and J. M. Oliveira, *J. Mater. Sci.: Mater. Med.*, 2020, **31**, 27.
43 A. Di Luca, K. Szlazak, I. Lorenzo-Moldero, C. A. Ghebes, A. Lepedda, W. Swieszkowski, C. Van Blitterswijk and L. Moroni, *Acta Biomater.*, 2016, **36**, 210–219.
44 A. Di Luca, B. Ostrowska, I. Lorenzo-Moldero, A. Lepedda, W. Swieszkowski, C. Van Blitterswijk and L. Moroni, *Sci. Rep.*, 2016, **6**, 22898.
45 W. Prananingrum, Y. Naito, S. Galli, J. Bae, K. Sekine, K. Hamada, Y. Tomotake, A. Wennerberg, R. Jimbo and T. Ichikawa, *Biomed. Mater.*, 2016, **11**, 015012.
46 N. Annabi, J. W. Nichol, X. Zhong, C. D. Ji, S. Koshy, A. Khademhosseini and F. Dehghani, *Tissue Eng., Part B*, 2010, **16**, 371–383.
47 M. Li, X. Fu, H. Gao, Y. Ji, J. Li and Y. Wang, *Biomaterials*, 2019, **216**, 119269.
48 S. Zhu, W. Jing, X. Hu, Z. Huang, Q. Cai, Y. Ao and X. Yang, *J. Biomed. Mater. Res., Part A*, 2017, **105**, 3369–3383.
49 M. C. Stewart, K. M. Saunders, N. Burton-Wurster and J. N. Macleod, *J. Bone Miner. Res.*, 2000, **15**, 166–174.
50 A. M. Bhosale and J. B. Richardson, *Br. Med. Bull.*, 2008, **87**, 77–95.
51 J. R. Yang, Y. B. Liu, L. He, Q. G. Wang, L. Wang, T. Yuan, Y. M. Xiao, Y. J. Fan and X. D. Zhang, *Acta Biomater.*, 2018, **74**, 156–167.
52 S. Daghighi, J. Sjollema, H. C. van der Mei, H. J. Busscher and E. T. J. Rochford, *Biomaterials*, 2013, **34**, 8013–8017.
53 Y. Liu, X. Chen, S. Li, Q. Guo, J. Xie, L. Yu, X. Xu, C. Ding, J. Li and J. Ding, *ACS Appl. Mater. Interfaces*, 2017, **9**, 23428–23440.
54 D. Wu, X. Chen, T. Chen, C. Ding, W. Wu and J. Li, *Sci. Rep.*, 2015, **5**, 11105.

55 C. J. March, B. Mosley, A. Larsen, D. P. Cerretti, G. Braedt, V. Price, S. Gillis, C. S. Henney, S. R. Kronheim and K. Grabstein, *Nature*, 1985, **315**, 641–647.
56 A. C. Ferguson-Smith, Y.-F. Chen, M. S. Newman, L. T. May, P. B. Sehgal and F. H. Ruddle, *Genomics*, 1988, **2**, 203–208.
57 P. Isomäki and J. Punnonen, *Ann. Med.*, 1997, **29**, 499–507.
58 P. C. Heinrich, I. Behrmann, S. Haan, H. M. Hermanns, G. Müller-Newen and F. Schaper, *Biochem. J.*, 2003, **374**, 1–20.
59 M. P. van den Borne, N. J. Raijmakers, J. Vanlauwe, J. Victor, S. N. de Jong, J. Bellemans, D. B. Saris and S. International Cartilage Repair, *Osteoarthr. Cartil.*, 2007, **15**, 1397–1402.
60 X. Guo, H. Park, S. Young, J. D. Kretlow, J. J. van den Beucken, L. S. Baggett, Y. Tabata, F. K. Kasper, A. G. Mikos and J. A. Jansen, *Acta Biomater.*, 2010, **6**, 39–47.
61 Y. Du, H. Liu, Q. Yang, S. Wang, J. Wang, J. Ma, I. Noh, A. G. Mikos and S. Zhang, *Biomaterials*, 2017, **137**, 37–48.
62 G. Tian, S. Jiang, J. Li, F. Wei, X. Li, Y. Ding, Z. Yang, Z. Sun, K. Zha, F. Wang, B. Huang, L. Peng, Q. Wang, Z. Tian, X. Yang, Z. Wang, Q. Guo, W. Guo and S. Liu, *Acta Biomater.*, 2021, **127**, 131–145.
63 H. Chen, J. Erndt-Marino, P. Diaz-Rodriguez, J. Kulwatno, A. C. Jimenez-Vergara, S. L. Thibeault and M. S. Hahn, *J. Biomed. Mater. Res., Part B*, 2019, **107**, 1056–1067.